N87-22215

INSTABILITY OF AN INTERSHAFT SQUEEZE FILM DAMPER IN A TWO-SPOOL ROTOR DYNAMICS SIMULATOR

R.G. Alderson
Garrett Corporation
Phoenix, Arizona 86010

ABSTRACT

An instability associated with an intershaft squeeze film damper is described. The squeeze film is located between the intershaft bearing outer race and the low-speed shaft of a five-bearing, two-spool test rig. The instability is dominated by response of the third system mode to destabilizing excitation of the type described by Hibner, et al. Installing a spring cage in place of the intershaft damper removes the instability and produces satisfactory performance throughout the operating range.

INTRODUCTION

Trends in advanced technology engines are toward significantly higher turbine inlet temperatures, higher work stages, increased thrust-to-weight ratios, greater durability requirements, and reduced life-cycle costs. These trends are producing departures from traditional rotor systems that have significant effects on system rotor dynamics.

One Garrett design in this area is a two-spool engine that uses an intershaft roller bearing to support the turbine end of the high-pressure (HP) spool. This eliminates the high-temperature structure otherwise needed to support the HP turbine-end bearing. However, the intershaft bearing is a path for nonsynchronous excitation not found in traditional configurations.

Shaft diameters are kept to a minimum in order that disk bores and bearing diameters will be minimized. These measures for improving disk low-cycle fatigue lives and bearing lives are accomplished without requiring the low-pressure (LP) spool to operate supercritically. Although many of the modes encountered in the operating range display some flexure, the synchronous flexural critical speeds of the LP rotor are outside of the operating range. However, nonsynchronous excitation of these modes by the HP rotor via the intershaft bearing needs to be considered.

Shafting technology for advanced propulsion engines has not yet progressed to the extent that satisfactory operation can be guaranteed in this regime on the basis of analytical predictions alone. Commitment of an advanced engine design to a configuration incorporating these features requires a program of testing with a rotor dynamics simulator.

The dynamics rig designed to simulate the engine dynamics is a two-spool, corotating system driven by air impingement. Figure 1 depicts the dynamic system in schematic form. Individual spools are separately controlled and driven. The LP spool is supported by three bearings, two straddling the simulated fan, with the third bearing aft of the simulated LP turbine. The HP spool is supported by two bearings, including the intershaft bearing that has the inner race carried by the HP rotor.

The rotor system is installed in a rigid frame, with the spring cages used as bearing supports simulating engine structural stiffnesses. Each of the four structure-supported bearings is provided with an unsealed squeeze film damper. Centering springs are not used.

Originally, a squeeze film damper was also used with the intershaft bearing. This feature was employed in an effort to exploit fully the benefits of squeeze film dampers in controlling unbalance. The oil film was formed between the outer race and a housing rotating with the LP spool. The subsequent need to eliminate a subsynchronous instability led to removal of this damper in favor of a spring cage.

Initial rig testing revealed subsynchronous whirl that appeared at a part-speed condition and persisted throughout the operating range. The instability did not grow to destructive proportions, probably due to relatively well-balanced rotors. It was the dominant feature of the rotor response, however, and unacceptable for engine operation.

The intent of this paper is to describe the characteristics of the instability, and to discuss the influence of the intershaft squeeze film damper.

EARLY TEST EXPERIENCE

Figure 2 shows the speed schedule followed in early tests to approximate engine conditions. Acceleration through the speed range revealed some system modes synchronous with the LP rotor, while others were synchronous with the HP rotor. Initially, the LP-synchronous modes tended to be more severe. But trim balancing effectively reduced all synchronous response to relatively low levels. Subsynchronous response also was observed, beginning at a part-speed condition and persisting throughout the speed range. Trim balancing was not effective in reducing the amplitude of the subsynchronous response.

Figure 3 is an RPM spectrum map that typifies the system response. This data was obtained from a proximity probe sensing displacement of the simulated HP turbine wheel. This spectrum map is identical in character to maps for the simulated HP compressor and LP turbine wheels. These similarities emphasize the dynamic coupling provided by the intershaft bearing. Proximity probe data from the simulated fan showed less prominent subsynchronous response, probably due to the combined effects of fan mass and LP shaft flexibility.

Figure 3 shows the main subsynchronous response near 120 Hz, with a secondary subsynchronous response near 60Hz. The maximum amplitude of the 120 Hz component is in the range of 0.10 to 0.15 mm (4 to 6 mil) peak-to-peak for the HP turbine, and about twice that for the LP turbine. The 120 Hz component displays an increasing trend from its initiation through maximum operational speed for the rig. This response is regarded as an instability. Although these subsynchronous whirl amplitudes are not a threat to rig integrity, the presence of an instability would not be tolerable for engine operation.

CHARACTERIZATION OF RESPONSE

Figure 4 combines Figures 2 and 3 with the results of undamped whirl speed calculations. The solid lines define system whirl frequencies for various whirl ratios (LP spin speed/system whirl speed). The analysis was done in the whirl frame of reference, and extended from zero whirl ratio (nonrotating system) through unity whirl ratio (LP unbalance excitation). Whirl ratios corresponding to HP unbalance excitation vary according to the speed schedule. At 100 percent speed, the whirl ratio corresponding to HP unbalance is between 0.5 and 0.6.

Figure 4 also shows that the analytical model is in reasonable correlation with the test data. Particularly prominent is the agreement between response peaks and calculated whirl speeds for LP unbalance excitation (unity whirl ratio). The first three mode shapes corresponding to LP unbalance excitation are shown in Figure 5. Amplitude and phase data from the various displacement transducers are consistent with these mode shapes. All three modes display

shaft flexure but are not dominated by it. Analysis shows that most of the strain energy in these modes results from support participation rather than shaft flexure.

Figure 4 suggests that the subsynchronous activity around 60 Hz and 120 Hz is associated with the first and third system modes, respectively. Figure 5 shows that these two modes (particularly mode 3) involve participation by the intershaft bearing and squeeze film damper.

INSTABILITY OF INTERSHAFT DAMPER

The intershaft bearing is installed with the inner race mounted on the HP rotor. The squeeze film is formed between the outer race and a housing that rotates with the LP rotor. The damper is of the open-end type. Following the approach of Hibner, Kirk, and Buono (Ref. 1), the intershaft damper was modeled by a solution of the Reynolds Equation:

$$\frac{1}{6}\left[\frac{1}{R^2}\frac{\partial}{\partial\theta}\left(\frac{h^3}{\mu}\frac{\partial P}{\partial\theta}\right)+\frac{\partial}{\partial Z}\left(\frac{h^3}{\mu}\frac{\partial P}{\partial Z}\right)\right] = (W_1+W_2-2\dot{\phi})\frac{\partial h}{\partial\theta}+2\frac{\partial h}{\partial t} \qquad (1)$$

Making the "short bearing" assumption permits the first term on the left to be neglected. For steady whirl in a circular orbit,

$$h = C\,(1+\varepsilon\cos\theta) \qquad (2)$$

as is shown in Figure 6.

Then (1) reduces to

$$\frac{\partial^2 P}{\partial Z^2} = -\frac{12\mu\varepsilon\sin\theta}{C^2\,(1+\varepsilon\cos\theta)^3}\,(W_L-\dot{\phi}) \qquad (3)$$

Assuming that the pressure is symmetric across the width of the squeeze film, (3) can be integrated to obtain the pressure distribution:

$$P(Z,\theta) = -\frac{6\mu(Z^2-\frac{L^2}{4})\,\varepsilon\sin\theta}{C^2\,(1+\varepsilon\cos\theta)^3}\,(W_L-\dot{\phi}) \qquad (4)$$

For the open-end damper, the circumferential pressure distribution is approximated by the "π-film" in which pressure is positive over half of the annulus and zero elsewhere. Two cases need to be considered in the integration of the pressure to obtain the radial and tangential damper forces. In the first case, the damper spin speed is less than the journal whirl rate. The opposite situation constitutes the second case.

Case 1 - $\dot{\phi} > W_L$, $P=0$ for $0 \le \theta \le \pi$

$$F_r = 2\int_{\pi}^{2\pi}\int_{0}^{\frac{L}{2}} P(Z,\theta)\cos\theta\, R\,d\theta\,dZ =$$

$$-\frac{2\mu RL^3}{C^2}\,\frac{\varepsilon}{(1-\varepsilon^2)^2}\,(\dot{\phi}-W_L) \qquad (5)$$

which tends to center the journal.

$$F_t = 2\int_{\pi}^{2\pi}\int_{0}^{\frac{L}{2}} P(Z,\theta)\sin\theta\, R\,d\theta\,dZ =$$

$$-\frac{\pi\mu RL^3}{2C^2}\,\frac{\varepsilon}{(1-\varepsilon^2)^{3/2}}\,(\dot{\phi}-W_L) \qquad (6)$$

which tends to oppose whirl (stabilizing).

Case 2 - $\dot{\phi} < W_L$, $P=0$ for $\pi \le \theta \le 2\pi$

$$F_r = \int_{0}^{\pi}\int_{0}^{\frac{L}{2}} P(Z,\theta)\cos\theta\, R\,d\theta\,dZ =$$

$$-\frac{2\mu RL^3}{C^2}\,\frac{\varepsilon^2}{(1-\varepsilon^2)^2}\,(W_L-\dot{\phi}) \qquad (7)$$

which tends to center the journal, as in Case 1.

$$F_t = \int_{0}^{\pi}\int_{0}^{\frac{L}{2}} P(Z,\theta)\sin\theta\, R\,d\theta\,dZ =$$

$$+\frac{\pi\mu RL^3}{2C^2}\,\frac{\varepsilon}{(1-\varepsilon^2)^{3/2}}\,(W_L-\dot{\phi}) \qquad (8)$$

which tends to promote whirl (destabilizing). This is the opposite of the effect noted in Case 1.

This analysis, together with the mode shapes shown in Figure 5, offers an interpretation of the system response shown in Figure 4. As the LP rotor is accelerated, LP-synchronous response in each of the first three system modes can be seen at LP speeds around 3300, 5000, and 7200 rpm. According to the analysis, intershaft damper forces due to LP-synchronous whirl are small since $\dot{\phi} \simeq W_L$. Simultaneously, HP-synchronous whirl is present due to excitation of the second and third system modes by the HP rotor. Excitation of the sixth mode probably occurs also. Stabilizing forces are developed in the intershaft damper due to HP-synchronous whirl since $\dot{\phi} > W_L$. Evidently these stabilizing forces, together with damping furnished by the grounded squeeze film dampers, are the dominant influences on system response.

For LP speeds above 8000 rpm, the character of the response changes. Following the expected sharp drop in LP-synchronous response as the LP rotor passes through the third system mode, a subsynchronous response appears around 120 Hz. The amplitude of the subsynchronous response continues to increase throughout the operating range. The unique feature of the third system mode (in contrast with the first and second modes) is the degree of participation of the intershaft damper. This is illustrated in Figure 5.

A plausible explanation of the response derives from the abundance of transients in the system. Noncircular damper orbits and the nonlinearity of squeeze film damper forces are primary sources of transients which ordinarily are of little consequence. Even though system response to transients will tend to include response in the system modes, system damping usually suppresses the transients immediately. But because the intershaft damper participates strongly in the third system mode, destabilizing forces become significant since $\dot{\phi} < W_L$ for this mode. It appears that the secondary subsynchronous response around 60 Hz that occurs in the same speed range as the 120 Hz instability is a similar but weaker phenomenon. Damper participation in the first system mode is significantly reduced compared with the third mode. Virtually no intershaft damper activity occurs in the second system mode, nor is there subsynchronous response associated with it.

REMOVAL OF INSTABILITY

A limited test program was undertaken in which various system parameters were modified in an attempt to remove the instability. These modifications included clearance changes in the intershaft damper, the HP compressor-end damper, and the LP turbine-end damper. Support stiffness at the LP turbine-end bearing also was varied. Significant reduction of subsynchronous response was not observed.

Removal of the instability was accomplished by refitting the test rig with a spring cage in place of the intershaft damper. The result of this modification is shown in Figure 7, an rpm spectrum map of the simulated HP turbine response after the refit. The subsynchronous responses that appeared previously above 8000 rpm are absent. Although a slightly different speed schedule was used in this test, many of the synchronous features identified previously can be seen. The speed schedule modification does not affect the validity of the test. The modified speed schedule was followed merely to give a better simulation of engine conditions than the schedule shown in Figure 2.

CONCLUSIONS

Use of a squeeze film damper in an intershaft application is responsible for the instability observed during testing of a two-spool rotor dynamics simulator. Replacing the intershaft

damper with a spring cage removed the instability. A limited program of testing alternate damper clearances and support stiffnesses revealed no significant effects on the instability. The instability was driven by destabilizing hydrodynamic forces in the intershaft damper that develop when the system tends to whirl at a speed less than the damper spin speed. The instability appears to be associated with the third system mode, in which the intershaft damper is influential.

NOMENCLATURE

C	Damper Radial Clearance
e	Eccentricity
F_r	Damper Oil Film Radial Force
F_t	Damper Oil Film Tangential Force
h	Damper Oil Film Thickness
P	Damper Oil Film Pressure
R	Damper Radius
t	Time
Z	Damper Axial Coordinate
ε	Eccentricity Ratio
θ	Angle From Line of Centers, In Direction of Rotation
μ	Oil Kinematic Viscosity
$\dot{\phi}$	Journal Whirl Rate
W_1	Inner Journal Spin Speed
W_2	Outer Journal Spin Speed
W_L	LP Rotor Spin Speed

REFERENCES

1 Hibner, D.H., Kirk, R.H., and Buono, D.F., "Analytical and Experimental Investigation of Intershaft Squeeze Film Dampers, Part I-Demonstration of Instability," Journal of Engineering for Power, Trans. ASME, Vol. 99, Series A, No. 1, Jan. 1977, pp. 47-52.

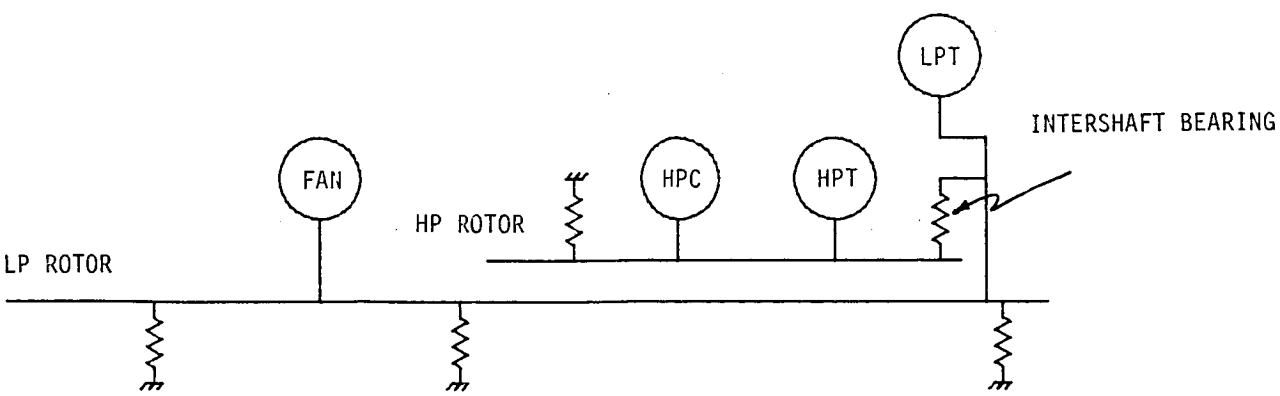

Figure 1. Rotor Dynamics Simulator Schematic.

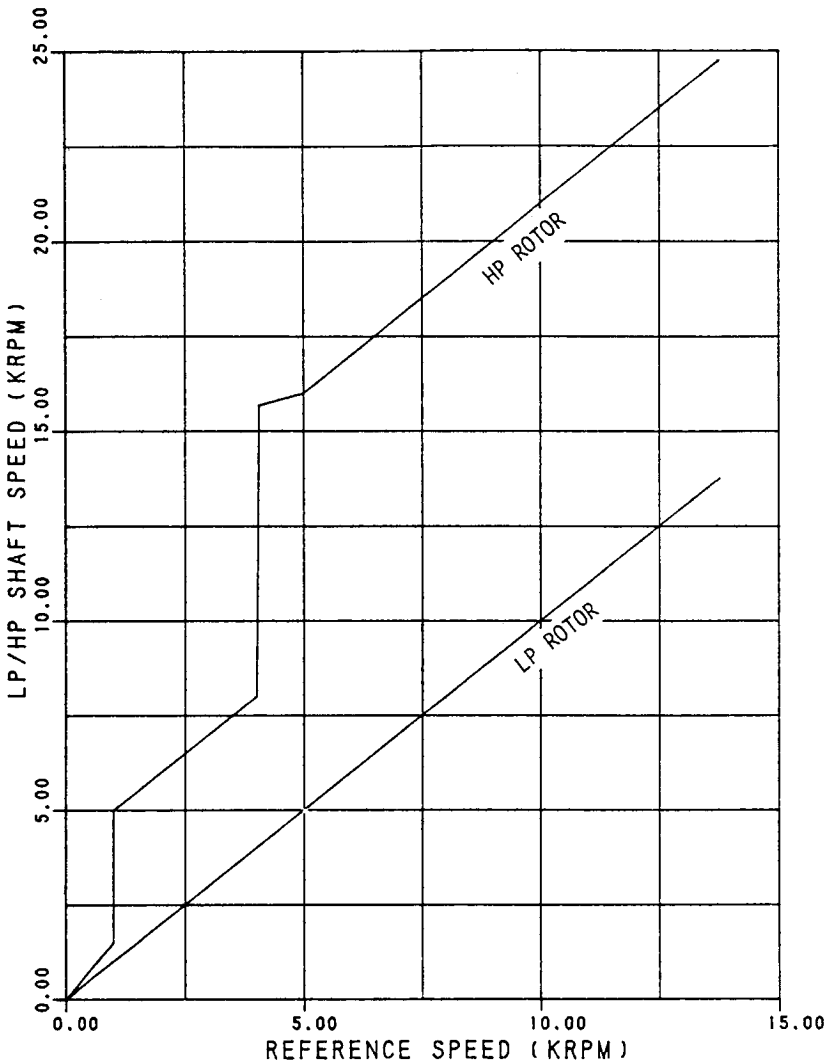

Figure 2. Rotor Dynamics Simulator Speed Schedule. System Includes Intershaft Squeeze Film Damper.

ORIGINAL PAGE IS
OF POOR QUALITY

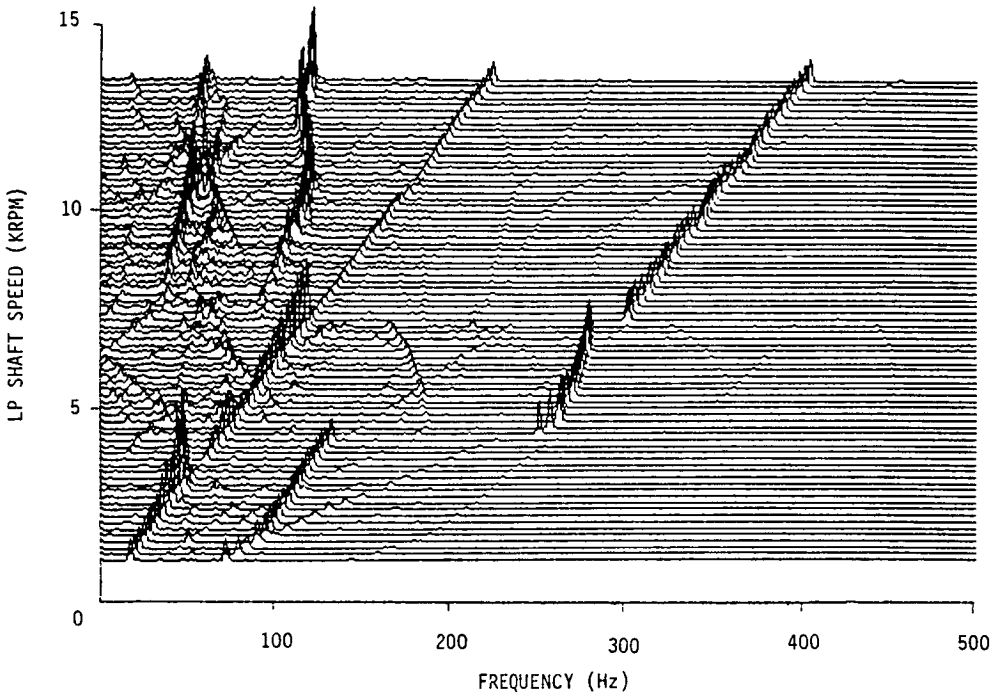

Figure 3. RPM Spectrum Map for Simulated HP Turbine.

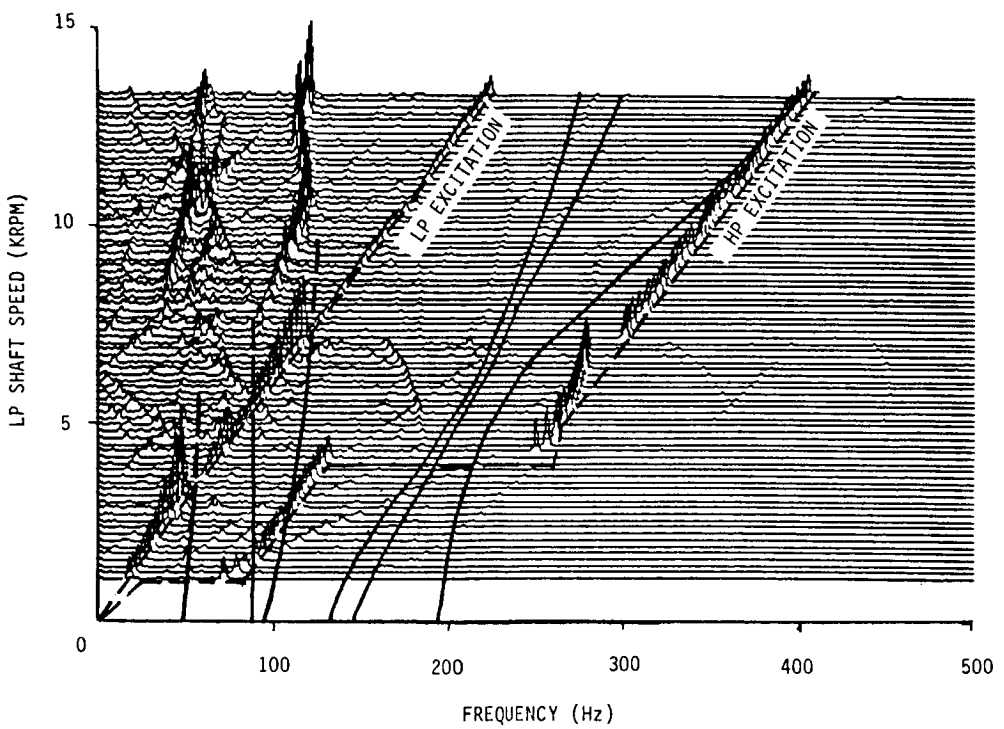

Figure 4. RPM Spectrum Map with Predicted Whirl Map Superimposed.

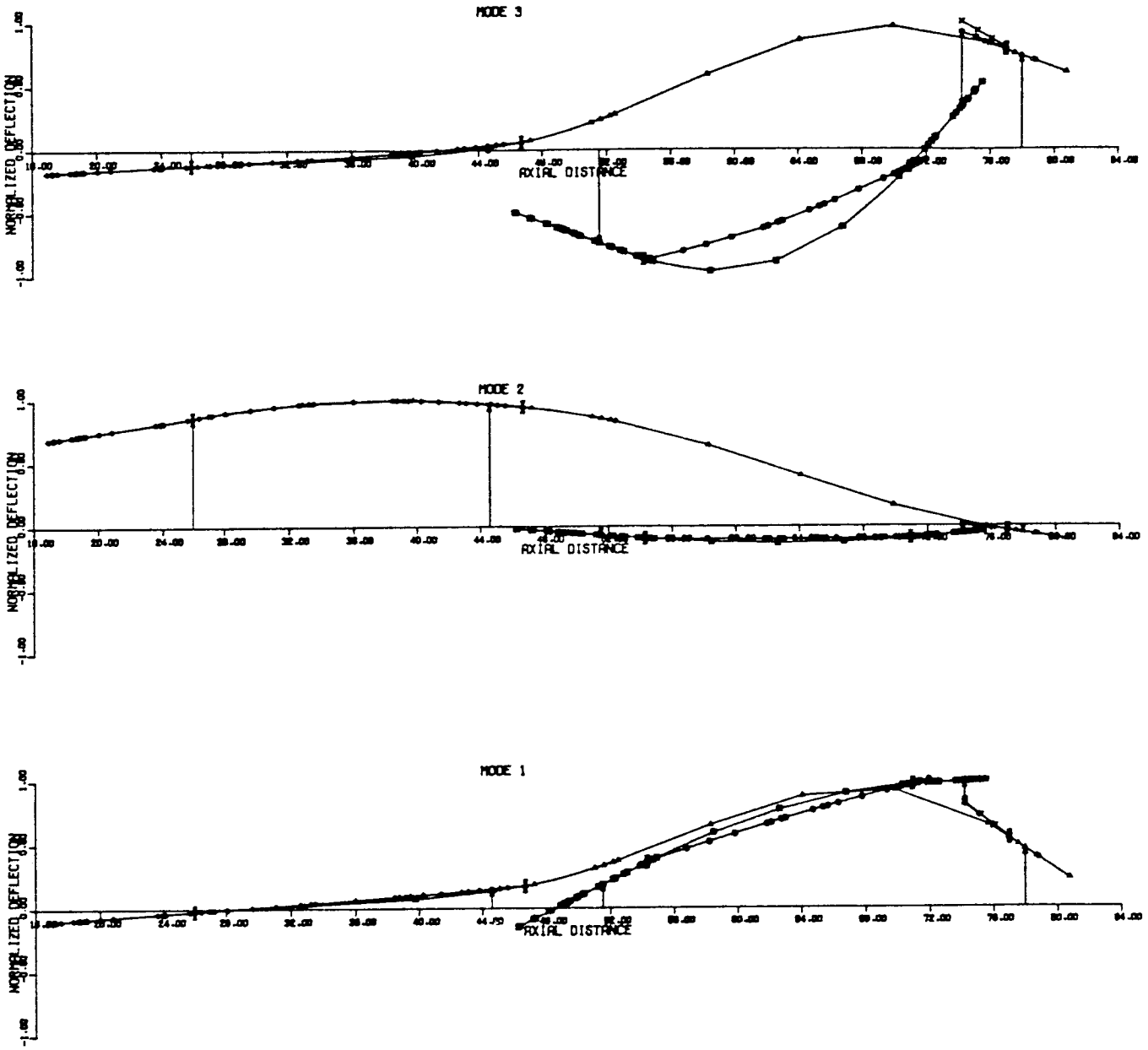

Figure 5. Deformed Shapes for System Modes 1 - 3.

ORIGINAL PAGE IS
OF POOR QUALITY

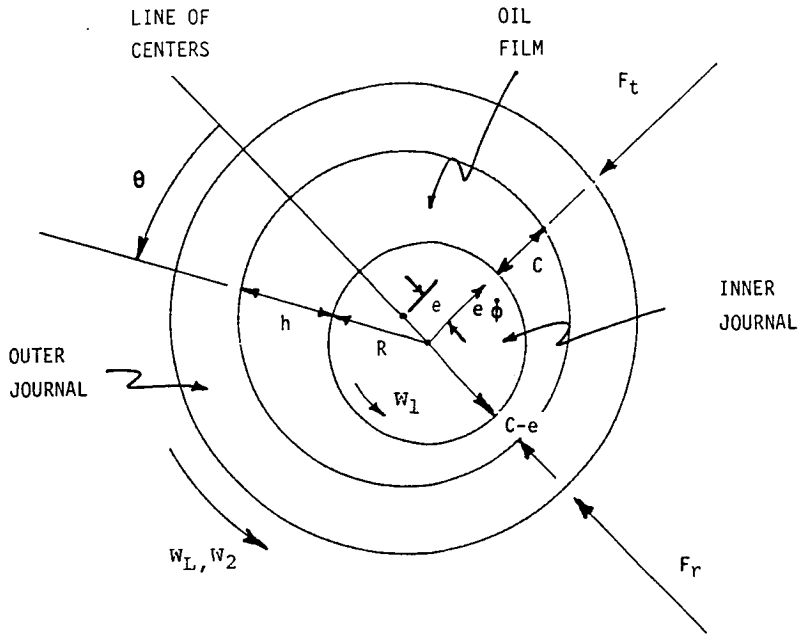

Figure 6. Intershaft Squeeze Film Damper Geometry.

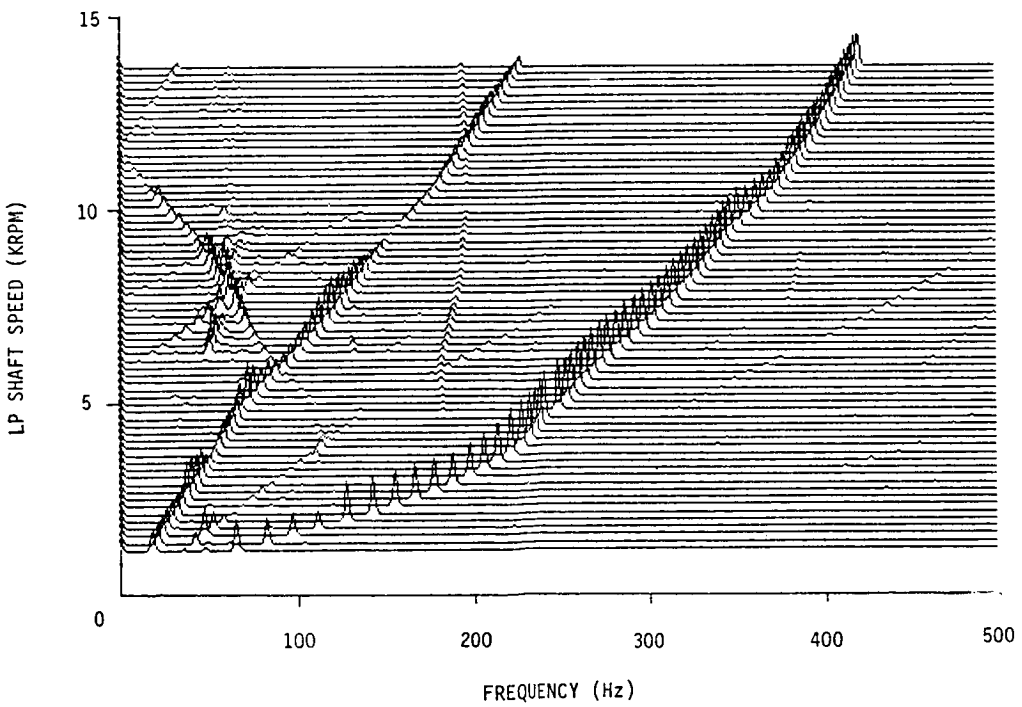

Figure 7. RPM Spectrum Map for Simulated HP Turbine.
Spring Cage Replaces Intershaft Squeeze Film Damper.